Journal of Alloys and Compounds 507 (2010) 42–46

Contents lists available at ScienceDirect

Journal of Alloys and Compounds

journal homepage: www.elsevier.com/locate/jallcom

Electrochemical impedance spectroscopy of HVOF-sprayed NiTi intermetallic coatings deposited on AISI 1045 steel

M.M. Verdian*, K. Raeissi, M. Salehi

Department of Materials Engineering, Isfahan University of Technology, Isfahan 84156-83111, Iran

ARTICLE INFO

Article history:
Received 26 May 2010
Received in revised form 3 July 2010
Accepted 8 July 2010
Available online 23 July 2010

Keywords:
Coating materials
Mechanical alloying
Intermeallics
X-ray diffraction
Corrosion
Electrochemical impedance spectroscopy

ABSTRACT

NiTi intermetallic coatings were sprayed on AISI 1045 steel substrate by using high velocity oxygen-fuel (HVOF) process. Polarization tests and electrochemical impedance spectroscopy (EIS) measurements were employed to study corrosion behavior of the coatings in 3.5% NaCl solution. Polarization tests indicated that the corrosion current densities of the HVOF coatings are comparable to those of NiTi alloys reported in the literature. On the other hand, EIS measurements showed that although the solution penetrates through the coating defects and causes to corrosion of the substrate, but, the corrosion performance of the coatings improves at long times due to the plugging of the defects by corrosion products which hinders higher attack of the substrate.

1. Introduction

Thermal spray procedures are coating processes in which feedstock materials are fed in powder or wire form. The coating materials are heated to a molten or semi-molten state and accelerated towards a substrate to form a dense, functional and protective overlay coating. The particles bond to the substrate mechanically and, in some cases, metallurgically. Thermal spray processes require minimal substrate preparation, can be applied in the field, and are low temperature (<200 °C) methods in comparison to techniques such as weld overlay. These processes are also versatile modern surfacing methods with regard to economics, range of materials and scope of applications. These processes permit the rapid application of high-performance materials in thickness from a few mils to more than 1 mm on parts of a variety of sizes and geometries [1]. Therefore, thermal spray coatings can provide protection against corrosion and wear failures. In this regard, high velocity oxy-fuel (HVOF) coatings are extensively used in industry to improve the corrosion and wear resistance of metallic surfaces [2,3].

HVOF process is a state-of-the-art process in which a liquid (kerosene) or gases (hydrogen or propane) fuel is employed for high energetic combustion with pure oxygen, applied at elevated pressure. The high energetic combustion allows a flame with a relatively low temperature and extremely high speed to be produced. This speed may reach values of 2000 m s^{-1}. The strongly expanding combustion gases accelerate the powder particles inserted in the combustion chamber to reach high velocity values (400–1000 m s^{-1}) in the deposition phase. This can result very dense and adherent coatings with little oxidation during the application [3]. Consequently, coatings with high corrosion resistance can be obtained by using HVOF [4].

Recently, NiTi coatings have been developed for corrosion and wear applications. In this regard, it was reported that the erosion resistance of NiTi coatings made by laser plasma hybrid spraying was approximately 40 times as high as that of Ti6Al4V alloy [5,6]. In addition, Chiu et al. reported that the cavitation and erosion–corrosion resistance of the laser-cladded NiTi coating was higher than that of AISI 316 stainless steel [7–9]. Also, it has been indicated that corrosion resistance of TIG [10] and laser-cladded [7–9] NiTi coatings is comparable to that of AISI 316 stainless steel.

Nevertheless, most of the used processes for application of NiTi coatings (e.g. laser cladding and laser plasma hybrid spraying) are expensive and have some limitations such as substrate geometry [4]. Hereon, HVOF process can be used as a technological alternative to the more expensive technologies. Guilemany et al. have developed HVOF NiTi coatings [11] who investigated the corrosion performance of thermally sprayed NiTi coatings on a carbon steel substrate. According to Tafel polarization tests, they concluded that HVOF NiTi coatings prepared from atomized powders showed fairly

* Corresponding author at: Department of Materials Engineering, Isfahan University of Technology, Isfahan 84156-83111, Iran. Tel.: +98 913 239 0787; fax: +98 311 391 2752.
E-mail address: m.verdianrizi@ma.iut.ac.ir (M.M. Verdian).

0925-8388/$ – see front matter © 2010 Elsevier B.V. All rights reserved.
doi:10.1016/j.jallcom.2010.07.132

good corrosion resistance. On the other hand, it has been reported that the polarization behavior of the HVOF NiTi coating prepared from mechanically alloyed powders can be similar to that of the coating prepared from atomized powders [12]. Verdian et al. have investigated the corrosion performance of HVOF NiTi coatings on 316L stainless steel substrate [13]. According to electrochemical impedance spectroscopy (EIS) measurements, they showed that HVOF NiTi coatings exhibited a good passive behavior during long-term immersion.

Long-term corrosion behavior of HVOF NiTi coatings on plain carbon steel substrate has not been reported in the literature. In the present work, the EIS measurements were used to evaluate the corrosion resistance of HVOF NiTi coatings on 1045 steel during long-term immersion.

2. Experimental procedures

2.1. Materials

Mechanically alloyed Ni–Ti powders with a particle size range of (−63 to +20 μm) were used in the experiments. The nominal composition of the powders was Ni-47.69% Ti-1.5% Fe-0.03% O (at.%). The feedstock materials were produced from elemental Ti and Ni powders by solid-state synthesis utilizing low energy mechanical alloying (MA) with times up to 100 h. In this regard, near equiatomic mixture of elemental powders of Ni (99.5 at.%, 50 μm) and Ti (98 at.%, 300 μm) were subjected to MA in a tumbler ball mill under argon atmosphere. Hardened steel vials and balls (10 mm diameter) were used for ball milling. The ball-to-powder weight ratio (BPR) was 40:1. The ball milling was conducted with the disk revolution speed of 85 rpm [14]. An AISI 1045 steel (Fe–0.46C–0.12Cr–0.12Ni–0.03Mo–0.79Mn–0.18Si–0.008P–0.03S wt.%) with the dimensions of 100 mm × 50 mm × 4 mm was used as the substrate material. Before spraying, the substrates were blasted with SiC grits to a surface roughness (Ra) of about 10 μm.

2.2. Thermal spray processes

A Met Jet III HVOF system (Metallisation Limited, Dudley, UK) was used to spray NiTi coatings. The kerosene was used as a liquid fuel. The gun was scanned vertically up and down at 80 mm s^{-1} to build up a coating of the required thickness. The interpass spacing was 3 mm. Typically, 8 passes of the thermal spray gun were employed to achieve deposits 150–200 μm thick. During and after the deposition, air jets were directed towards the back of the substrates to provide cooling and maintain the substrate temperature below 200 °C. The substrate temperature was monitored by thermocouples placed on the rear of the plates. Details of the spraying parameters used to produce HVOF coatings are given in Table 1.

2.3. Characterization of the powders and coatings

Powders and coatings were analyzed by X-ray diffraction (XRD, Philips X'Pert-MPD) using Cu Kα radiation (λ = 1.54056 Å) generated at 40 kV and 30 mA. For microstructural examination, a cross-section of each coating was prepared and polished up to 1 μm diamond suspension. The coatings were etched with a HF:HNO_3 solution (10 mL HF, 25 mL HNO_3, 150 mL H_2O) to reveal the microstructure and afterwards were observed in a scanning electron microscope (SEM, Philips XL30) operated at 20 kV equipped with an EDS tool for microanalysis.

2.4. Corrosion tests

For corrosion tests, the coated specimens were wet ground up to 1200 grit SiC paper. Then, they were washed in distilled water and ethanol. Finally, they were dried in warm air. Mini-corrosion cells were constructed by sticking open glass tubes with 0.8 cm diameter on the samples. Tafel polarization tests were conducted in a three-electrode system after 1 h immersion. The counter electrode was a platinum wire and the reference electrode was a standard calomel electrode (SCE). The tests were performed in 3.5% NaCl solution using an AMETEK potentiostat (model PARSTAT 2273) at scan rate of 1 mV s^{-1}. The corrosion potentials as well as corrosion current densities were extracted from the plots using Tafel extrapolation method.

Electrochemical impedance spectroscopy (EIS) measurements were also performed using the mentioned corrosion cell and equipment. Impedance values were recorded in the frequency range from 100 kHz to 10 mHz. The voltage amplitude was 10 mV with respect to the open circuit potential. The analysis of the spectra was performed using Zview software. After 14 days of immersion, the cross-sections of corroded specimens were examined by using SEM.

Table 1
HVOF process parameters.

Spray parameters	Unit
Stand off distance	35 cm
Oxygen flow rate	840 L/min
Kerosene flow rate	240 mL/min
Nozzle length	20 cm
Powder feed rate	60 g/min
Carrier gas (N_2) flow rate	3 L/min

3. Results and discussion

3.1. Characterization of powders and coatings

The XRD patterns of powders and coatings are shown in Fig. 1. A broad diffraction peak at the Bragg angles of 41–45° indicates the presence of an amorphous/nanocraystalline phase in feedstock powders [12–15]. The studies of HVOF coating revealed that the peaks belonging to NiTi (austenite phase), Ni_4Ti_3, Ni and also $NiTiO_3$ exist in the respective XRD pattern. The formation of Ni_4Ti_3 phase as a metastable precipitate has been previously reported during air plasma spraying of NiTi alloys [15]. The Ni phase is formed either due to crystallization of amorphous phase or preferential oxidation of Ti element during the spraying process [12,15]. Formation of Ni has been previously reported in HVOF spraying of NiTi intermetallic powders [11,12]. It is speculated that $NiTiO_3$ is likely to have formed due to the oxidation of NiTi particles during the spraying process [12,13].

SEM micrographs from the cross-sections of HVOF coating are shown in Fig. 2. From these figures it is found that the coating has low porosity. Also, it is well-bonded to substrate with no distinctive irregular interface (Fig. 2a). In Fig. 2b, two regions are visible in the microstructure of the coating; a bright matrix and some dark stringers. For characterization of these regions, six EDS point measurements were performed on each region. The results indicated that the bright matrix is a region with chemical composition close to 50Ni–50Ti (49.6 ± 1.6 Ni, 49.3 ± 1.2 Ti, 0.8 ± 0.3 Fe at.%) and the dark stringers are the high-oxygen containing regions (9 ± 1.6 Ni, 83 ± 1.2 Ti, 10 ± 1 O at.%). It seems that the bright matrix of the coatings contains NiTi and Ni_4Ti_3 and the dark stringers contain $NiTiO_3$. Incidentally, Ni_4Ti_3 precipitates are too small to detect by SEM [12,13,15].

3.2. Corrosion behavior

3.2.1. Tafel polarization tests

Fig. 3 shows the Tafel polarization (E-log i) plots of HVOF NiTi coatings and steel substrate in 3.5% NaCl solution in room temperature at static and natural aerated conditions. The values of the corrosion potential (E_{corr}) and corrosion current density (i_{corr}) are extracted from the curves using Tafel extrapolation method.

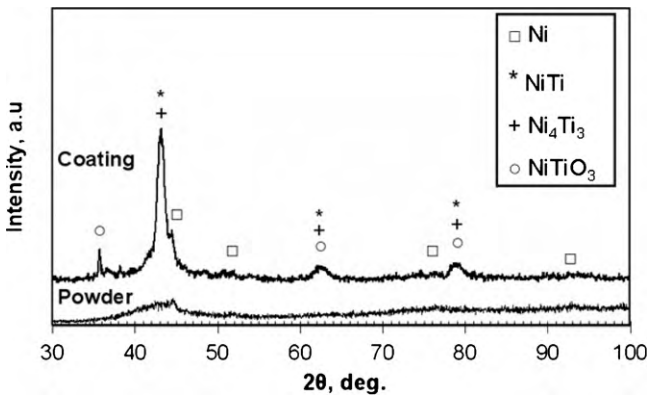

Fig. 1. XRD patterns of feed stock powder and HVOF coating.

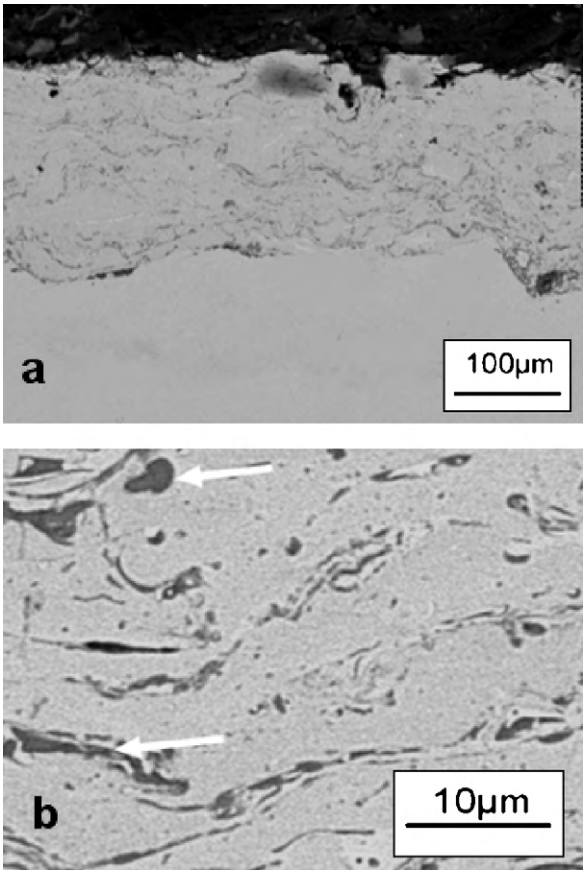

Fig. 2. SEM micrographs of sections from HVOF coating; (a) at lower magnification and (b) at higher magnification.

The E_{corr} and i_{corr} values are the average of three polarization measurements. In this regard, the E_{corr} values were −0.41 and −0.62 V_{SCE} for HVOF coating and steel substrate, respectively. It is clear that the corrosion potential values of steel substrate are more negative than those of NiTi coatings. It means that the substrate is more active than the NiTi, and thus, substrate corrosion can take place in preference to the coating [11,16].

The i_{corr} values were 0.6 and 13 μA cm^{-2} for HVOF coating and steel substrate, respectively. It should be mentioned that the corrosion current density of the present coating is comparable to that of bulk NiTi samples (0.2–0.8 μA cm^{-2}) provided in the literature [9,10]. As seen in Tafel plots (Fig. 3), the coating shows passive behavior. The polarization curve of the coating exhibits a breakdown at higher anodic potentials, around 0 V_{SCE}. It was demonstrated that the passivity of NiTi alloys is due to the formation of TiO_2 surface film [11–13]. Moreover, the passivity breakdown potential is greater than 0.2 V_{SCE} for bulk NiTi alloys [9,10,12]. It can be concluded that the passive behavior of the present HVOF coating is inferior to that of bulk NiTi alloys. It seems that the presence of secondary phases, i.e. Ni_4Ti_3, Ni and $NiTiO_3$ (Fig. 1) in the HVOF coating hinders the formation of a homogeneous passive layer. The corrosion process can be preferentially initiated along phase boundaries, possibly due to the microgalvanic corrosion [12,13]. This phenomenon can limit the passive behavior of the coating and lead to shift the surrounding metal from passive to active state [12,13]. A similar behavior was observed for laser-cladded NiTi coatings [9]. I was reported that the passive behavior of the laser-cladded NiTi coatings is inferior to that of the bulk NiTi alloy due to the presence of defects and inhomogeneities arising from melting, solidification and overlapping tracks in laser processing [9].

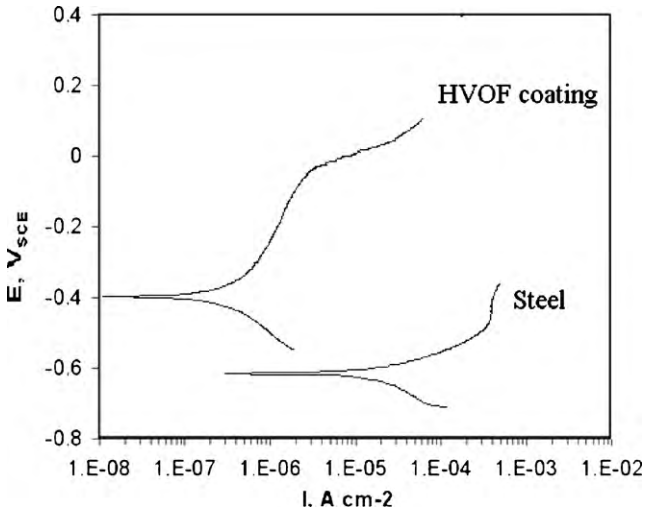

Fig. 3. Polarization curves of steel substrate and HVOF coating in 3.5% NaCl solution.

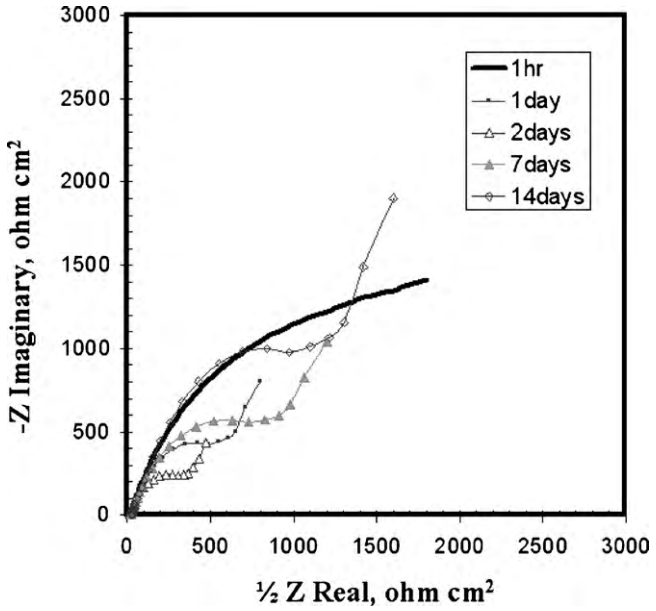

Fig. 4. Experimental Nyquist diagram for HVOF coated sample in 3.5% NaCl at different times of exposure.

Similar corrosion results were obtained by Guilemany et al. [11] for HVOF NiTi coatings on low-alloyed carbon steel substrate. Based on Tafel polarization results, they concluded that the HVOF coatings exhibited a slight passive-like behavior. It would seems that the polarization behavior of the present HVOF coating is similar to that of the polished HVOF coating examined by Guilemany et al. [11], i.e. they seem to possess similar polarization curves, similar E_{corr}, i_{corr} and passivity breakdown potential. It means that the corrosion resistance of the HVOF NiTi coating prepared from mechanically alloyed powders can be similar to that of the coating prepared from atomized powders.

3.2.2. Electrochemical impedance spectroscopy of the coatings

Figs. 4 and 5 show the Nyquist and Bode phase plots of HVOF coated steel at various immersion times, respectively. After 1 h of exposure, one capacitive loop is evident on Nyquist plot (Fig. 4), and accordingly, one inflection point on corresponding Bode phase plot (Fig. 5). It means that the system shows one time constant. This high-frequency loop could be physically related to the coating

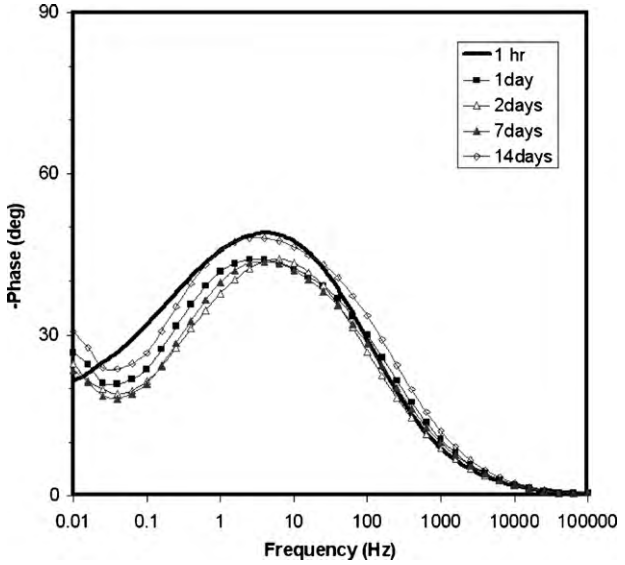

Fig. 5. Bode phase plot of HVOF coated sample measured over the different immersion periods.

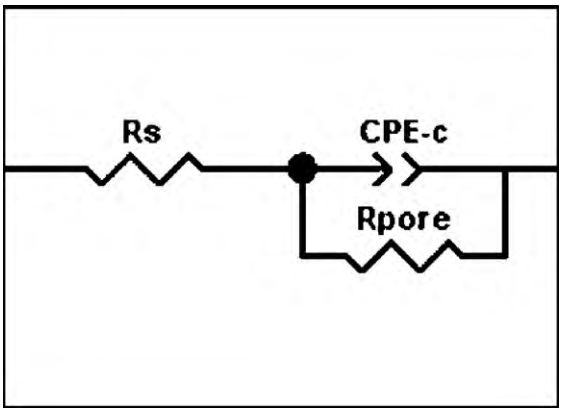

Fig. 6. Equivalent circuit for HVOF coated sample after 1 h immersion.

characteristics [13,17]. This electrochemical cell can be modeled by a simple equivalent circuit which consists of the electrolyte resistance R_e and the dielectric property of the coating represented by a pair of elements of CPE-c and R_{pore} (Fig. 6). This behavior has been seen in several coating systems in which the coating is very dense and can form a passive layer such as HVOF-sprayed stainless steel coating [17], hydrothermal deposited TiO_2 [18] and HVOF-sprayed WC-CoCr coating [19] in 3.5% NaCl solution.

Furthermore, after 1-day of exposure, the style of the Nyquist and Bode phase plots was changed. As seen in Nyquist plots (Fig. 4), the high-frequency capacitive loop has become smaller indicating the decrease in R_{pore}; a straight line also appears at low frequencies. The straight line appears due to the *Warburg impedance* created when charge transfer is influenced by a semi-infinite length diffusion process [20,21]. This feature appears as a result of diffusion of

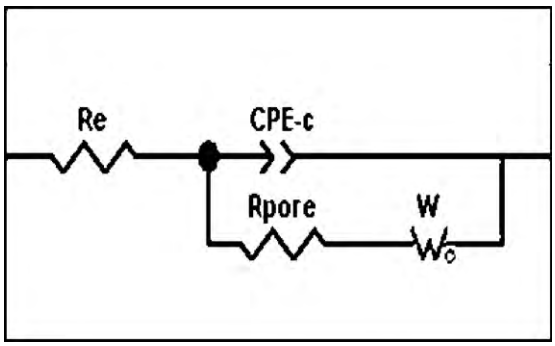

Fig. 7. Equivalent circuit for HVOF coated sample for immersion times longer than 1-day.

electrolyte through the coating defects such as splat boundaries or pores [17]. On the other hand, after 7 days of exposure, the high-frequency capacitive loop has become larger indicating the increase in R_{pore}. This feature arises probably as a result of local accumulation of corrosion products in the defects, which increases the pore resistance due to the blocking of defects by corrosion products [13,22]. In this condition, the equivalent circuit shown in Fig. 7 is useful for describing the electrochemical cell [21]. The equivalent circuit consists of the electrolyte resistance R_e; the dielectric property of the coating presented by a pair of elements, CPE-c (c means coating) and *Warburg element*, *W*.

Table 2 summarizes the circuit parameters using the fitting circuit in Figs. 6 and 7. After 1 h immersion, E_{OCP} value is $-0.43\,V_{SCE}$ which decreases with the increase of immersion time (after 2 days, E_{OCP} is $-0.58\,V_{SCE}$). On the other hand, *Warburg* impedance increased and R_{pore} decreased with the increase of immersion time (times up to 2.days). These two phenomena show that the electrolyte penetrates through the coating defects [13]. But, after 7 days, E_{OCP} value was raised to $-0.49\,V_{SCE}$. This trend continued until 14 days in which E_{OCP} value reached to $-0.41\,V_{SCE}$. Also, *Warburg* impedance decreased and R_{pore} increased with the increase of immersion time (times up to 14 days). This feature arises most likely as a result of local accumulation of corrosion products in the defects, which increases the pore resistance due to the blocking of defects. This phenomenon is also called "plugging effect" by some authors [13,22].

The SEM micrograph from the surface of HVOF coating after 14 days immersion is shown in Fig. 8a. A surface pore can be observed in this figure (as shown by a circle). The high magnification micrograph of this pore is shown in Fig. 8b. The corrosion products are visible inside the pore. The EDX analysis showed that corrosion products contain oxygen and iron. It seems that this pore has been plugged by corrosion products formed due to corrosion of substrate.

The SEM micrograph of the cross-section of the coating after 14 days of immersion is shown in Fig. 9. No obvious indication of blistering and delamination of the coating can be observed. However, the substrate seems to be locally attacked at the substrate/coating interface. It has been demonstrated that the penetration of electrolyte through the coating defects can strongly affect the electrochemical behavior of thermal spray coatings. The

Table 2
Electrochemical parameters obtained from EIS spectra of HVOF coated sample.

Exposed time	E_{ocp} (V SCE)	R_e ($\Omega\,cm^2$)	CPE-c ($\mu F\,cm^{-2}$)	η_{CPE-c}	R_{pore} ($\Omega\,cm^2$)	W ($\mu\,cm^{-2}\,\Omega^{-1}\,s^{-0.5}$)
1 h	−0.43	39	420	0.63	4494	–
1-day	−0.50	40	506	0.62	1567	2248
2 days	−0.58	44	570	0.65	897	3308
7 days	−0.49	40	397	0.61	2047	321
14 days	−0.41	45	276	0.63	3451	90

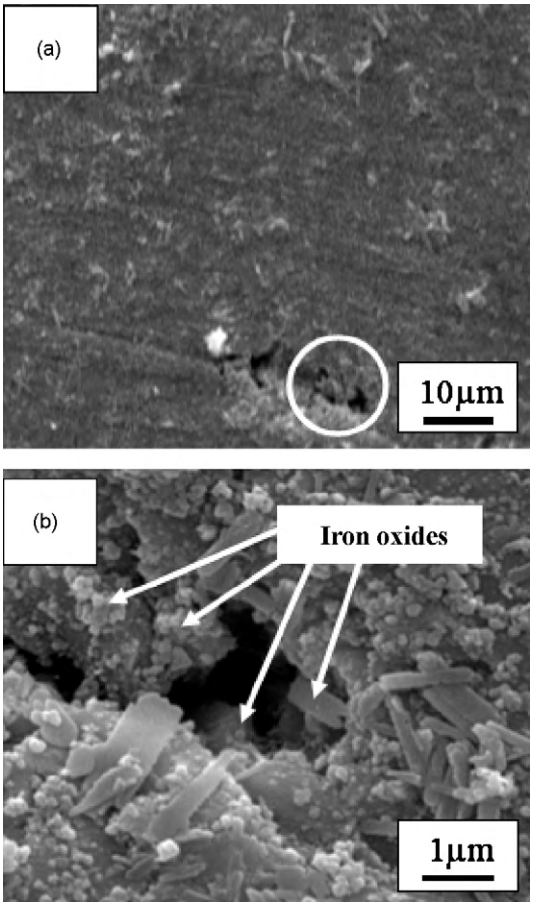

Fig. 8. (a) SEM micrograph from surface of HVOF coating after 14 days immersion (a surface pore has been shown by a circle) and (b) high magnification SEM micrograph of the pore.

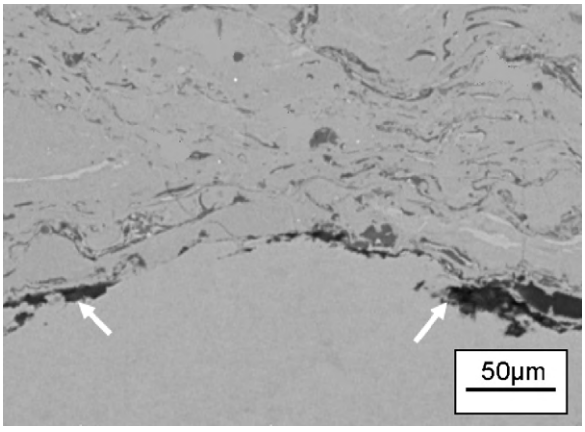

Fig. 9. SEM micrograph of the cross-section of HVOF coating after 14 days immersion (arrows show attacked regions of the substrate).

coating defects are mainly used by the electrolyte to reach the base steel. In this case, if the electrolyte reaches a less noble substrate, a galvanic pair can be formed with a consequent steel attack, coating depletion and loss of surface properties [11,23,24].

According to EIS measurements of HVOF NiTi coatings on 1045 steel substrate, it can be seen that the corrosion mechanism is not the same at earlier stage and later stage of immersion. It seems that the surface oxidation is the main corrosion mechanism of coatings at early stages of immersion while the electrolyte penetration through the coating defects is the main responsible of the electrochemical response evolution with increase of immersion time (Figs. 4 and 5). It is expected that when the electrolyte reaches the substrate causes its corrosion and changes the impedance response [24]. As a consequence, the coatings have a high corrosion resistance for short immersion times, but the corrosion resistance of the coatings decreases with time. On the other hand, the corrosion performance of coatings can improve at longer times due to the plugging of the defects by corrosion products which hinders higher attack of the substrate.

4. Conclusion

1. NiTi-base coatings were deposited on 1045 steel. Tafel polarization tests indicated that corrosion current densities of the HVOF coating are comparable to that of NiTi alloys reported in the literature.
2. The EIS experiments showed that although the solution penetrates through the coating defects and causes to corrosion of the substrate, but, the corrosion performance of the coatings improves at long times due to the plugging of the defects by corrosion products which hinders higher attack of the substrate.
3. It seems that the surface oxidation is the main corrosion mechanism of coatings at early stages of immersion while the electrolyte penetration through the coating defects is the main responsible of the electrochemical response evolution with increase of immersion time.

References

[1] H. Herman, S. Sampath, R. McCune, MRS Bull. 25 (2000) 17–25.
[2] E. Celik, I. Ozdemir, E. Avcic, Y. Tsunekawa, Surf. Coat. Technol. 193 (2005) 297–302.
[3] D. Zhang, S.J. Harris, D.G. McCartney, Mater. Sci. Eng. A 344 (2003) 45–56.
[4] L. Fedrizzi, L. Valentinelli, S. Rossi, S. Segna, Corros. Sci. 49 (2007) 2781–2799.
[5] H. Hiraga, T. Inoue, H. Shimura, A. Matsunawa, Wear 231 (1999) 272–278.
[6] H. Hiraga, T. Inoue, S. Kamado, Y. Kojima, A. Matsunawa, H. Shimura, Surf. Coat. Technol. 139 (2001) 93–100.
[7] K.Y. Chiu, F.T. Cheng, H.C. Man, Mater. Sci. Eng. A 407 (2005) 273–281.
[8] K.Y. Chiu, F.T. Cheng, H.C. Man, Mater. Sci. Eng. A 392 (2005) 348–358.
[9] K.Y. Chiu, F.T. Cheng, H.C. Man, Surf. Coat. Technol. 200 (2006) 6054–6061.
[10] F.T. Cheng, K.H. Lo, H.C. Man, Surf. Coat. Technol. 172 (2003) 316–321.
[11] J.M. Guilemany, N. Cinca, S. Dosta, A.V. Benedetti, Corros. Sci. 51 (2009) 171–180.
[12] M.M. Verdian, M. Salehi, K. Raeissi, Surf. Eng. (2010), doi:10.1179/026708410X12593178265823.
[13] M.M. Verdian, K. Raeissi, M. Salehi, Corros. Sci. 52 (2010) 1052–1059.
[14] M.M. Verdian, M. Salehi, K. Raeissi, Int. J. Mod. Phys. B 24 (10) (2010) 1261–1269.
[15] M.M. Verdian, M. Salehi, K. Raeissi, Surf. Eng. (2010), doi:10.1179/026708409X12490360425927.
[16] J.M. Guilemany, J. Fernández, J.M. de Paco, J. Sanchez, Surf. Eng. 14 (2) (1998) 133–135.
[17] J.M. Guilemany, J. Fernández, N. Espallargas, P.H. Suegama, A.V. Benedetti, Surf. Coat. Technol. 200 (2006) 3064–3072.
[18] F.T. Cheng, P. Shi, H.C. Man, Surf. Coat. Technol. 187 (2004) 26–32.
[19] M. Magnania, P.H. Suegamaa, A.A. Cândido Recco, J.M. Guilemany, C.S. Fugivara, A.V. Benedetti, J. Mater. Res. 10 (4) (2007) 377–385.
[20] C. Liu, Q. Bi, A. Matthews, Corros. Sci. 43 (2001) 1953–1961.
[21] F. Mansfeld, M.W. Kendig, J. Electrochem. Soc. 135 (1988) 828–833.
[22] Y. Wang, W. Tian, T. Zhang, Y. Yang, Corros. Sci. 51 (2009) 2924–2931.
[23] M.M. Verdian, M. Salehi, K. Raeissi, Surf. Eng. (2010), doi:10.1179/026708410X12506870724398.
[24] J.M. Guilemany, N. Espallargas, P.H. Suegama, A.V. Benedetti, Corros. Sci. 48 (2006) 2998–3013.